Structural impact on the eigenenergy renormalization for carbon and silicon allotropes and boron nitride polymorphs

Roxanne Tutchton, Christopher Marchbanks, and Zhigang Wu

Phys. Rev. B **97**, 205104 — Published 7 May 2018

DOI: 10.1103/PhysRevB.97.205104

Structural impact on the eigenenergy renormalization for carbon and silicon allotropes and boron nitride polymorphs

Roxanne Tutchton, Christopher Marchbanks, and Zhigang Wu*
Department of Physics, Colorado School of Mines, Golden, CO 80401, USA
(Dated: March 19, 2018)

The phonon-induced renormalization of electronic band structures is investigated through first-principles calculations based on the density functional perturbation theory for nine materials with various crystal symmetries. Our results demonstrate that the magnitude of the zero-point renormalization (ZPR) of the electronic band structure is dependent on both crystal structure and material composition. We have performed analysis of the EPC induced renormalization for two silicon (Si) allotropes, three carbon (C) allotropes, and four boron nitride (BN) polymorphs. Phonon dispersions of each material were computed, and our analysis indicates that materials with optical phonons at higher maximum frequencies, such as graphite and hexagonal BN, have larger absolute ZPR's, with the exception of graphene, which has a considerably smaller ZPR despite having phonon frequencies in the same range as graphite. Depending on the structure and material, renormalizations can be comparable to the GW many-body corrections to Kohn-Sham eigenenergies and, thus, needs to be considered in electronic structure calculations. The temperature dependence of the renormalizations is also considered, and in all materials, the eigenenergy renormalization at the band gap and around the Fermi level increases with increasing temperature.

I. INTRODUCTION

The effects of electron-phonon coupling (EPC) on electronic structure has been an integral area of study since the inception of the quantum theory of solids. EPC is the primary mechanism behind superconductivity and the thermal dependence of the electrical resistivity in metals; it leads to the optical absorption by the indirect gap in semiconductors such as silicon, the temperature-dependence of the band gap, the distortion of electronic band structures, and hot carrier thermalization, and it is one of the dominant factors determining the carrier mobility in semiconductors.[1] In current first-principles electronic structure calculations, the electron-electron interaction responsible for the quasiparticle (QP) excitation can be quantitatively described by the *GW* approximation,[2–4] and the *GW* band gaps (E_{g}) agree with experimental data for many semiconductors to within a few tenths of an eV. However, the electron-phonon interaction involved in the QP excitation has been largely ignored. This is because the QP eigenenergy shifts ($\Delta\varepsilon_{n\mathbf{k}}$) due to lattice vibrations in common semiconductors are often less than 100 meV, which is well within the margin of error for the current *GW* approximation methods.

The *GW* approximations are usually performed in addition to density functional theory (DFT[5,6]) calculations within the local density approximation (LDA) or the generalized gradient approximation (GGA) in order to provide many-body corrections to the KS eigenenergies and band gaps. In certain materials, $\Delta\varepsilon_{n\mathbf{k}}$ and the resulting band gap renormalization, ΔE_{g}, are comparable to the corresponding many-body corrections, such that the electron-phonon renormalization is significant to electronic-structure calculations. For example, the lattice vibrations at 0 K, or zero-point renormalization (ZPR), of the direct band gap of diamond is ~ 0.4 eV,[7] which, compared to the *GW* correction of 2.04 eV, is non-negligible. Furthermore, EPC may also depend on the crystal structures of allotropes and polymorphs: for instance, nanoscale materials[8] or structures under high pressures may have enhanced EPC (as with well-known, high pressure induced superconductivity) despite the fact that the ΔE_{g} in these materials is negligible for their bulk counterparts under ambient conditions.

Early calculations performed by Allen and Cardona[9,10] using rigid-ion pseudopotentials approximations and empirical phonon models (Weber's bond-charge model), demonstrated that both Fan Migdal (Eq.3) and Debye Waller (Eq.4) self energy contributions are significant in determining the band gap renormalization in Si and germanium (Ge). King-Smith *et al.* used a self consistent DFT method to perform one of the first parameter free calculations of the temperature dependence of the band gap of Si. Rigorous first-principles calculations[7,11–18] of $\Delta\varepsilon_{n\mathbf{k}}$ based on density functional perturbation theory (DFPT[19,20]) emerged in late 2000s. Giustino *et al.*[11,13] implemented Allen-Heine theory[21] calculations based on the EPW[22]), QUANTUM ESPRESSO[23], and WANNIER90[24] codes[11,25], while Poncé *et al.*[7,17,18] used the Allen-Heine-Cardona (AHC) formalism in the ABINIT package,[26] which uses the Sternheimer[27] method that allows the summation in equations 3 and 4 to be limited to occupied bands. This drastically decreases the burden of computational convergence. Another implementation[12,15,16] was incorporated into the Yambo code.[28] Like Giustino's[13] method (which we will call the QE+EWP method for convenience), the Yambo implementation uses QUANTUM ESPRESSO[23] as its base DFT package. Poncé *et al.*[17] have compared the ZPR's of eigenenergies in diamond obtained from ABINIT and QE+Yambo and found that the discrepancy between the two codes was less than 4 meV.

Other first-principles approaches to evaluate $\Delta\varepsilon_{n\mathbf{k}}$ in-

clude the frozen phonon (FP) method, which has been used to examine the accuracy of the harmonic adiabatic approximation[18,29] as well as to evaluate the significance of many-body effects on EPC.[30] The FP approach suffers from the necessity of untenably large supercells for long-wavelength phonon modes; however, the intuitive aspect of the method makes it attractive for calculations using smaller **q**-point grids. More recently, a deterministic supercell method to phonon-induced band gap renormalization has been explored by Zacharias and Giustino,[31] in which they use the theory of Willams[32] and Lax[33] to study the temperature dependence of the band gaps of silicon, diamond, and gallium arsenide. The perturbative G_0W_0 approximation is another method used to improve the accuracy of $\Delta\varepsilon_{n\mathbf{k}}$ calculations. It has been used in concert with the FP approach to compare the renormalization results from perturbative DFT[30] as well as incorporate GW corrections into the EPC calculations for nanostructures, such as fullerene C_{60}.[34] In their comparison of FP, DFT, and GW calculations of the ZPR of diamond, Antonius *et. al.*[30] found that the perturbative G_0W_0 corrections resulted in a roughly 200 meV increase in the magnitude of ΔE_{g} at the Γ-point, indicating that GW corrections are a significant factor in accurate ZPR calculations. The G_0W_0 approximation was also recently implemented in a study by Monserrat to calculate electron-phonon coupling strength for several materials including diamond and silicon.[35] As the goal of this study is to compare and analyze EPC indued renormalizations for a large number of structures, we have not included GW corrections due to time and computational constraints.

Nonadiabatic corrections are also a key factor in $\Delta\varepsilon_{n\mathbf{k}}$ and ΔE_{g} calculations as discussed in section II B. Comparisons of adiabatic and nonadiabatic effects on ΔE_{g} calculations have been performed by Antonius *et. al.*[29] and Poncé *et al.*[7] These studies focus on semiconductors and the semiconducting band gap. The results suggest that certain materials, such as polar materials, or materials with a non-zero Born effective charge, are not well described by the adiabatic approximation and, thus, require a nonadiabatic correction. Poncé *et al.*[7], in particular, have performed extensive convergence studies on the adiabatic and nonadiabatic methods for various semiconductors and insulators. They also used fitting techniques to predict the convergence of the ZPR as the broadening parameter, $i\eta$, approaches zero, which yielded larger renormalizations for polar materials than were previously calculated by Antonius *et. al.*[29]

In this article we study the effects of crystal structure and dimensionality on EPC from first-principles. Using isoelectronic C and Si allotropes and BN polymorphs as prototypical examples, we show that the zero-point renormalization of the electronic eigenenergies around the Fermi energy can be reduced or enhanced when the crystal structure or dimension is modified. A total of nine structures were examined: diamond Si, quasi-2D buckled silicene, diamond, graphite, graphene, zincblende BN (z-BN), wurtzite BN (w-BN), layered hexagonal BN (h-BN), and 2D hexagonal BN (2D-BN). In addition to the ZPR, we examined the temperature dependence of $\Delta\varepsilon_{n\mathbf{k}}$ and ΔE_{g} and the relationship between the ZPR and phonon dispersion. Our results suggest that it becomes necessary to examine the phonon spectrum and renormalization of electronic band structures when new bulk crystal structures or new nanostructures are proposed with computational materials design.

In section II we will briefly summarize the theory and current computational methods for calculating the phonon renormalization of QP energies using both the adiabatic approximation (sec.II A) and the nonadiabatic corrections (sec.II B) to AHC theory. In appendix A we discuss the electronic structure calculations of each of the considered materials. Results of the renormalization convergence tests are given in section III. In section IV we present and discuss the ZPR and temperature-dependent electronic band structures for C allotropes (diamond, graphite, and graphene) and BN polymorphs (zinc blend, wurtzite, layered hexagonal, and single layer) calculated from the adiabatic and nonadiabatic treatments of AHC theory, followed by concluding remarks in section V.

II. THEORY AND METHODOLOGY

In this section, we briefly review the formalism of Allen-Heine-Cardona theory in the adiabatic approximation and a nonadiabatic correction the AHC theory. The notation and derivations below are summarized from Giustino *et al.*[1]

A. Allen-Heine-Cardona theory

Allen and Heine[21] laid out the theoretical framework for the temperature dependence of electronic band structures based on second order perturbation theory in the adiabatic and harmonic approximations. An effective study of these treatments requires the use of the Fan-Migdal (FM) and Debye-Waller (DW) electron self-energies where the shift in a particular energy level is defined by

$$\Delta\varepsilon_{n\mathbf{k}} = \Delta^{\mathrm{FM}}\varepsilon_{n\mathbf{k}} + \Delta^{\mathrm{DW}}\varepsilon_{n\mathbf{k}}, \tag{1}$$

where $\varepsilon_{n\mathbf{k}}$ is the eigenenergy of the state with band n and wave vector $\mathbf{k}$. The FM self-energy, $\Delta^{\mathrm{FM}}\varepsilon$, is the dynamic correction to the electronic excitation energies. It derives its name from the 1951 work done by Fan[36] and the work done by Migdal in 1958,[37] but it is most often referred to as either the Fan term[9,21,38] or the Migdal term.[39,40] For continuity, the names are combined in recent literature.[1] The Fan-Migdal term describes the dynamic polarization of the lattice, and it is obtained by multiplying the first-order perturbation terms to recover the energy shift due to the second-order atomic displacement. The second term in equation 1 is commonly called

the Debye-Waller electron self-energy, $\Delta^{\mathrm{DW}}\varepsilon$, due to its similarities to the factor of the same name associated with temperature dependent x-ray diffraction spectra. This is a static term that describes the difference between the total potential for an interacting system and the potential for the same system with its nuclei clamped at equilibrium.[1] In other words, it is the result of the second-order perturbation due to lattice vibrations in the potential.

The theory developed by Allen and Heine[21] relies on two approximations: first is the implementation of the Rayleigh-Schrödinger approximation and, second, the assumption that the phonon energies associated with the FM self-energy are negligible.[1] Then, using translational invariance of the thermal shift, Allen and Heine expressed both the FM and DW corrections in terms of the first order perturbations of the self-consistent potential via the electron-phonon matrix elements,

$$g_{mn\nu}(\mathbf{k},\mathbf{q}) = \langle u_{m\mathbf{k}+\mathbf{q}} | \Delta_{\mathbf{q}\nu} v^{KS} | u_{n\mathbf{k}} \rangle, \tag{2}$$

where $\Delta_{\mathbf{q}\nu} v^{KS}$ is the scattering potential. These matrix elements describe scattering of an electron from one Bloch state ($n\mathbf{k}$), to another Bloch state ($m\mathbf{k}+\mathbf{q}$), with phonon of frequency $\omega_{\mathbf{q}\nu}$.

The self-energy terms are then expressed as

$$\Delta^{\mathrm{FM}}\varepsilon_{n\mathbf{k}} = \sum_{m\neq n,\nu} \int \frac{d\mathbf{q}}{\Omega_{\mathrm{BZ}}} \frac{(2n_{\mathbf{q}\nu}+1)\left|g_{mn\nu}(\mathbf{k},\mathbf{q})\right|^2}{\varepsilon_{n\mathbf{k}} - \varepsilon_{m\mathbf{k}+\mathbf{q}} + i\eta}, \tag{3}$$

$$\Delta^{\mathrm{DW}}\varepsilon_{n\mathbf{k}} = -\sum_{m\neq n,\nu} \int \frac{d\mathbf{q}}{\Omega_{\mathrm{BZ}}} \frac{(2n_{\mathbf{q}\nu}+1)[g^{\mathrm{DW}}_{mn\nu}(\mathbf{k},\mathbf{q})]^2}{(\varepsilon_{n\mathbf{k}} - \varepsilon_{m\mathbf{k}} + i\eta)} \tag{4}$$

Here $n_{\mathbf{q}\nu}$ is the Bose-Einstein occupation factor for the phonon frequency associated with phonon $\mathbf{q}$ and branch ν (Eq. 10) and Ω_{BZ} denotes the volume of the Brillouin zone. The small imaginary term, $i\eta$, in both the FM and DW terms is added as a computational method to smooth the self-energy functions and speed convergence of the energy shifts. In a majority of studies, $i\eta$ is set to 100 meV to account for the finite lifetimes of the electronic states defined by the imaginary part of the self-energy[7,13,29,30]. In equation 4, the DW electron-phonon matrix element, $g^{\mathrm{DW}}_{mn,\nu}(\mathbf{k},\mathbf{q})$, is an effective matrix element approximated from the products of standard electron-phonon matrix elements (Eq. 2)[1,13]:

$$[g^{\mathrm{DW}}_{mn,\nu}(\mathbf{k},\mathbf{q})]^2 = \frac{1}{2\omega_{\mathbf{q}\nu}} \sum_{\kappa\alpha,\kappa'\alpha'} t^{\nu}_{\kappa\alpha,\kappa'\alpha'}(\mathbf{q}) h^*_{mn,\kappa\alpha}(\mathbf{k}) h_{mn,\kappa'\alpha'}(\mathbf{k}), \tag{5}$$

where

$$t^{\nu}_{\kappa\alpha,\kappa'\alpha'}(\mathbf{q}) = \frac{e_{\kappa\alpha\nu}(\mathbf{q}) e^*_{\kappa\alpha'\nu}(\mathbf{q})}{M_\kappa} + \frac{e_{\kappa'\alpha\nu}(\mathbf{q}) e^*_{\kappa'\alpha'\nu}(\mathbf{q})}{M_{\kappa'}}, \tag{6}$$

$$h_{mn,\kappa\alpha}(\mathbf{k}) = \sum_{\nu} (M_\kappa \omega_{0\nu})^{1/2} e_{\kappa\alpha\nu}(0) g_{mn\nu}(\mathbf{k},0). \tag{7}$$

In the above expressions, $e_{\kappa\alpha\nu}(\mathbf{q})$ are phonon eigenvectors of the dynamical matrix with atomic species κ, Cartesian direction α, and phonon branch ν.

Combining the FM and DW self-energy terms, as dictated by equation 1, the temperature dependent eigenenergy shift is

$$\Delta\varepsilon_{n\mathbf{k}} = \sum_{m\neq n,\nu} \int \frac{d\mathbf{q}}{\Omega_{\mathrm{BZ}}} \left[\sum_m \frac{\left|g_{mn\nu}(\mathbf{k},\mathbf{q})\right|^2}{\varepsilon_{n\mathbf{k}} - \varepsilon_{m\mathbf{k}+\mathbf{q}} + i\eta} - \frac{[g^{\mathrm{DW}}_{mn\nu}(\mathbf{k},\mathbf{q})]^2}{(\varepsilon_{n\mathbf{k}} - \varepsilon_{m\mathbf{k}} + i\eta)} \right] (2n_{\mathbf{q}\nu}+1), \tag{8}$$

and the renormalized eigenenergy is

$$E_{n\mathbf{k}} = \varepsilon_{n\mathbf{k}} + \Delta\varepsilon_{n\mathbf{k}}. \tag{9}$$

The temperature dependence in equation 8 resides entirely in the Bose-Einstein factor, where

$$n_{\mathbf{q}\nu} = \frac{1}{e^{\frac{\hbar\omega_{\mathbf{q}\nu}}{k_B T}} - 1}. \tag{10}$$

In order to determine the eigenenergy shifts at zero temperature, we set $T = 0$, and the Bose-Einstein factor vanishes. The remaining energy shift, $\Delta\varepsilon^{ZP}_{n\mathbf{k}} = \Delta\varepsilon_{n\mathbf{k}}(T = 0)$, is the "zero-point renormalization" or ZPR.

Equation 8 is the adiabatic formulation of eigenenergy renormalization based on the initial work of Allen and Heine[21]. Later this theory was developed into a computational method by Allen and Cardona[9,10]. Thus, the literature generally refers to the complete formalism as the Allen-Heine-Cardona (AHC) theory. The theory is limited by its use of Rayleigh-Schrödinger perturbation theory and static treatment of the electronic screening. This is insufficient for certain materials including metals, semi-metals, and polar materials, thus, in the next section (II B), we discuss the nonadiabatic correction the AHC theory.

B. Nonadiabatic corrections to Allen-Heine-Cardona theory

The Born-Oppenheimer,[41] or adiabatic approximation, treats phonons as static perturbations such that the interatomic force constants are calculated for electrons in the ground state, resulting in a phonon-frequency independent electronic screening. This approximation is effective for insulators and large gap semiconductors in which the band gap is much larger than the phonon energy; however, for narrow-gap semiconductors, semimetals, metals, and polar materials variations in adiabatic and nonadiabatic phonon energies become significant at the center of the BZ. This is due to the phonon behavior in the region around $\mathbf{q} = 0$, where the nonadiabatic phonon energy correction is comparable to the adiabatic phonon energy.[1,42,43] In this case, the static perturbation approximation fails and a dynamic correction, which does not neglect the phonon frequencies ($\omega_{\mathbf{q}\nu}$) in the FM self-energy, is used.

The effects of nonadiabatic vibrational frequencies were first investigated in the works of Lazzeri and Mauri[44] and Pisana *et al.*[45] They performed calculations in the adiabatic approximation on a particular phonon branch of graphene then added a nonadiabatic frequency renormalization derived from the phonon self-energy. Around the same time, studies were done on metallic single-walled carbon nanotubes (CNT) that confirmed the importance of nonadiabatic effects for such materials around $\mathbf{q} = 0$.[46,47] A broader study of nonadiabatic renormalizations was done for a variety of graphite intercalation compounds by Saitta *et al.*[42] where they found that the nonadiabatic results were in much better agreement with experiments than the adiabatic calculations. Two years later Calandra *et al.*[43] published complete phonon dispersions calculated with nonadiabatic corrections, which confirmed that nonadiabatic effects are most significant for small $\mathbf{q}$.

In addition to certain metals and semi-metals, EPC in polar materials is not adequately described by the adiabatic approximation. The difficulty arises from the existence of the polar singularity in the electron-phonon matrix elements, which results in a divergence of the FM term as $|\mathbf{q}| \to 0$.[1] Antonius *et al.*[29] have explored the effects of a dynamic correction to energy band renormalizations for several materials including diamond and zincblende BN. Using a similar method, Poncé *et al.*[7] have done a thorough study on the convergence issues arising from the computational adiabatic and nonadiabatic methods of calculating the ZPR in polar and nonpolar materials. The same formalism used for their study is implemented in ABINIT package,[26] and is the method we have used to calculate nonadiabatic corrections to the electronic band-structure renormalization.

A full treatment of the nonadiabatic electron self-energy requires the Green's function formalism of the Hedin-Baym equations summarized by Giustino.[1] However, it is not currently possible to perform self-consistent calculations using this method, so for practical, *ab initio* calculations, DFT or the GW method is used to obtain an approximate nonadiabatic correction. These approximations result in the following self-energy expressions as described by Giustino:[1]

$$\Delta\varepsilon^{\mathrm{FM}}_{nn'\mathbf{k}}(\omega) = \frac{1}{\hbar}\sum_{m\nu}\int \frac{d\mathbf{q}}{\Omega_{\mathrm{BZ}}} g^{*}_{mn\nu}(\mathbf{k},\mathbf{q}) g_{mn'\nu}(\mathbf{k},\mathbf{q}) \times \left[\frac{1 - f_{m\mathbf{k}+\mathbf{q}} + n_{\mathbf{q}\nu}}{\omega - \varepsilon_{m\mathbf{k}+\mathbf{q}}/\hbar - \omega_{\mathbf{q}\nu} + i\eta} + \frac{f_{m\mathbf{k}+\mathbf{q}} + n_{\mathbf{q}\nu}}{\omega - \varepsilon_{m\mathbf{k}+\mathbf{q}}/\hbar + \omega_{\mathbf{q}\nu} + i\eta}\right] \tag{11}$$

$$\Delta\varepsilon^{\mathrm{DW}}_{nn'\mathbf{k}} = \sum_{\nu}\int \frac{d\mathbf{q}}{\Omega_{\mathrm{BZ}}} g^{\mathrm{DW}}_{nn'\nu}(\mathbf{k},\mathbf{q},-\mathbf{q})(2n_{\mathbf{q}\nu}+1) \tag{12}$$

Here $n_{\mathbf{q}}$ is, again, the Bose-Einstein factor of equation 10 and

$$f_{n\mathbf{k}} = \frac{1}{e^{\frac{(\varepsilon_{n\mathbf{k}} - \varepsilon_F)}{k_B T}} + 1}. \tag{13}$$

is the Fermi-Dirac factor derived from the Fermi-Dirac distribution. The combination of equations 11 and 12. Gives the total eigenenergy correction

$$\begin{aligned} E_{n\mathbf{k}} = \varepsilon_{n\mathbf{k}} &+ \frac{1}{\hbar}\sum_{\nu}\int \frac{d\mathbf{q}}{\Omega_{\mathrm{BZ}}} \sum_{m} g^{*}_{mn\nu}(\mathbf{k},\mathbf{q}) g_{mn'\nu}(\mathbf{k},\mathbf{q}) \\ &\times \left[\frac{1 - f_{m\mathbf{k}+\mathbf{q}} + n_{\mathbf{q}\nu}}{\omega - \varepsilon_{m\mathbf{k}+\mathbf{q}}/\hbar - \omega_{\mathbf{q}\nu} + i\eta} + \frac{f_{m\mathbf{k}+\mathbf{q}} + n_{\mathbf{q}\nu}}{\omega - \varepsilon_{m\mathbf{k}+\mathbf{q}}/\hbar + \omega_{\mathbf{q}\nu} + i\eta}\right] \\ &+ \sum_{\nu}\int \frac{d\mathbf{q}}{\Omega_{\mathrm{BZ}}} g^{\mathrm{DW}}_{nn'\nu}(\mathbf{k},\mathbf{q},-\mathbf{q})(2n_{\mathbf{q}\nu}+1), \end{aligned} \tag{14}$$

known as the "nonadiabatic extension" of the AHC theory in equations 8 and 9.[1,7] The expression is tempera-

ture and frequency dependent. The ZPR is regained by setting $T = 0$, as was done at the end of section II B.

C. Calculation parameters and methods

First-principles calculations were performed using the ABINIT[26] DFT pseudopotential-plane-wave approach and the dynamic DFPT method with Sternheimer equations.[27] The GGA-PBE[48] was adopted for the exchange-correlation functional. We have used Troullier-Martins[49] pseudopotentials, generated using the Fritz-Haber code[50], and written in the FHI format. Energy cutoffs of 30 Ha for diamond, graphene, and 2D-BN, 40 Ha for graphite and hexagonal BN (h-BN), and 35 Ha for zincblende BN (z-BN) and wurtzite BN (w-BN) were necessary for convergence. Optimized lattice parameters and electronic structures were calculated for each material using $8 \times 8 \times 8$ **k**-mesh for the bulk materials and a $12 \times 12 \times 1$ **k**-mesh for 2D-BN, graphene, and silicene. For the phonon dispersions, linear response calculations were done using a $12 \times 12 \times 12$ **k**-mesh for the bulk materials and a $20 \times 20 \times 1$ **k**-mesh for the 2D structures. The coarse **q**-point grids used in the phonon dispersion calculations were $12 \times 12 \times 12$ and $6 \times 6 \times 6$ for the diamond bulk structures and hexagonal bulk structures, respectively. Likewise, **q**-point grids of $20 \times 20 \times 1$ were used for the 2D structures in order to accommodate the difficult convergence of the acoustic phonon branches. Fine **q**-point grids of $24 \times 24 \times 24$ and $40 \times 40 \times 1$ were used for the 3D and 2D materials, respectively.

For graphene and, particularly, graphite, it was necessary to include van der Waals corrections to the exchange-correlation energy. According to Mounet and Marzari,[51] DFT within standard LDA and GGA does not accurately predict the interlayer interactions dependent on van der Waals dispersion forces. These forces are known to be present in graphite, therefore, we have applied the vdw-DFT-D3(BJ) correction, with Becke-Johnson dampening, developed by Grimme.[52,53] This correction greatly improved the calculated interlayer distance for graphite compared with experimental measurements, and it led to more accurate phonon dispersions in both graphite and graphene as well.[51,54] Calculations of the lattice constants for graphite, as well as the other structures considered in this study, are given in Table III.

Using AHC formalism, as well as nonadiabatic corrections implemented in ABINIT and its corresponding post-processing programs,[7] the convergence of the ZPR, $\Delta\varepsilon^{ZP}_{n\mathbf{k}}$, was tested for each structure. Linear response calculation were performed using **k**-point grids of $8 \times 8 \times 8$ for all bulk materials and $12 \times 12 \times 1$ for all 2D structures. Sternheimer equations[27] were employed to limit the necessary number of bands needed to converge equations 8 and 14 to 18 bands for the bulk and 2D structures. We tested convergence for homogeneous **q**-point grids of up to $34 \times 34 \times 34$ for diamond and zincblende BN; up to $24 \times 24 \times 24$ for wurtzite BN, h-BN, and graphite; and up to $60 \times 60 \times 1$ for the monolayer structures, graphene, silicene, and 2D-BN. An imaginary smearing parameter of $i\eta = 100$ meV was used for each structure, following Poncé *et al.*[17] and Giustino, *et al.*'s[13]) to speed convergence of summation in Equations (8) and (14). Thorough investigations into the effects of this smearing parameter are explored in Poncé *et al.*[7] and Antonius *et al.*[29]

III. ZPR CONVERGENCE TESTS

We performed calculations to test the convergence of the eigenenergy renormalizations for each of the structures discussed above. This section describes the results of our tests to converge the total zero-point renormalizations of the energy bands nearest the Fermi level or at the band gap. We define this quantity as

$$\Delta E^{ZP}_{\mathrm{g}} = \Delta\varepsilon^{ZP}_{\mathrm{VB}} + \Delta\varepsilon^{ZP}_{\mathrm{CB}}, \tag{15}$$

where $\Delta\varepsilon^{ZP}_{\mathrm{VB}}$ is the ZPR of the valence band (VB), and $\Delta\varepsilon^{ZP}_{\mathrm{CB}}$ is the ZPR of the conduction band (CB). For the considered semiconductors with non-zero E_g, we calculated the total ZPR at the band gap, $\Delta E^{ZP}_{\mathrm{g}}$. For the semimetals with $E_g = 0$, we calculated the total ZPR around the Fermi energy, $\Delta\varepsilon^{ZP}_{\mathrm{VB}} + \Delta\varepsilon^{ZP}_{\mathrm{CB}}$, which we will call $\Delta E^{ZP}_{\mathrm{g}}$ for convenience despite the fact that there is not a true band gap in the case of the semimetals. Details of the computational methods and parameters are given in section II C. Convergence tests were performed for each structure using an imaginary smearing of $i\eta = 100$ meV in the denominators of equations 8 and 14 to speed convergence and mitigate computational demand.

A. ABINIT ZPR convergence tests for 3D and 2D structures

Figure 1 summarizes our ZPR convergence tests for each Si and C allotrope and BN polymorph using the ABINIT[26] implementation. We have calculated the total ZPR of the semiconductor band gap for Si, diamond, z-BN, w-BN, h-BN, and 2D-BN. In the cases of graphite, graphene, and silicene, where $E_g = 0$, we calculate the total ZPR around the Fermi energy. All ZPR calculations for the convergence tests were done at the Γ-point using the nonadiabatic corrections to AHC theory.

At least 500 irreducible q-wavevectors are required to reach satisfactory convergence in the 3D materials [Fig. 1 (a)]. The 2D structures, on the other hand, start to converge with around 300 q-wavevectors [Fig. 1 (b)]. For each material, we have calculated $\Delta E^{ZP}_{\mathrm{g}}(\Gamma)$ values converged to within 3-5 meV, and the final results are listed in Table I along with the VB and CB eigenenergy shift components. These convergence results are consistent with those of similar materials.[17] Both adiabatic and nonadiabatic calculations were done for each structure, but because the adiabatic approximation breaks down for

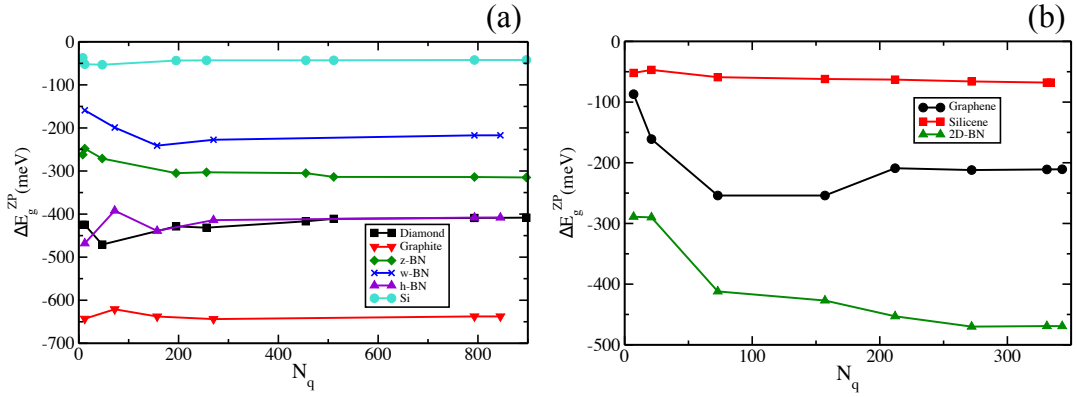

FIG. 1. The ZPR convergence tests using the nonadiabaitc AHC treatment for (a) the 3D structures (Si, diamond, graphite, z-BN, w-BN, and h-BN) and (b) 2D structures (silicene, graphene, and 2D-BN) at the Γ point. Renormalization values of are given as a function of the number of q-points in increasingly large homogeneous **q**-point grids of up to $34 \times 34 \times 34$ for the diamond-like structure, $24 \times 24 \times 24$ for w-BN and h-BN, and $60 \times 60 \times 1$ for the 2D structures.

the polar BN materials,[7] the data in Figure 1 were obtained using the nonadiabatic formulation, as it is valid for all of the materials considered.

The convergence of EPC eigenenergy renormalizations is notoriously difficult. Due to our use of the smoothing parameter $i\eta = 100$meV, the convergence calculations shown in Figure 1 are relatively quick, but they still require extremely dense homogeneous **q**-point grids. However, the computation of each energy band shift relies on the outcomes of consecutive first-principles calculations: the structural relaxation, linear response calculations, computation of the phonon eigenmodes and frequencies, the EPC and electron-phonon matrix-elements, and finally the calculation of the FM and DW self-energies. There are numerous possible methods to perform each of these steps as well as small numerical errors from associated approximations that become amplified in later calculations. The calculation protocol, pseudopotentials, and approximations all factor into the variations in results for the total ZPR of a given structure.

In 2014, Poncé *et al.*[17] conducted a study to compare several methods, different pseudopotentials, and convergence techniques used to calculate the direct gap renormalization of diamond. They showed that the resulting ZPR is sensitive to each of these aspects. Different formalisms or methods, such as FP and DFPT, can yield different ZPR values across the band structure. Likewise, the use of different pseudopotentials and exchange-correlation functional approximations produced variations as large as 50 meV in ZPR, as can the size of the **q**-point sampling. In present calculations, we employed homogeneous **q**-meshes, which, combined with the imaginary broadening parameter, $i\eta$, result in quicker convergence and smaller variations in ZPR values than random q-wavevector sampling.[17] Large random **q**-meshes can also be used, to aid in extrapolation. This is often done using Wannier functions to reduce the computational burden.[11] In 2015, Poncé *et al.*[7] performed ZPR convergence tests in the adiabatic and nonadiabatic formulations of AHC theory using interpolation methods to test the convergence behavior as the **q**-mesh goes to infinity and the $i\eta$ goes to zero. Due to this difference in technique, their results for certain materials (z-BN in particular) differ from other DFT results (Table II).

TABLE I. The calculated zero-point renormalization (in meV) of the CB, VB, and $\Delta E_{\rm g}^{ZP}$ at the Γ-point.

	Adiabatic			nonadiabatic		
Materials	$\Delta\varepsilon_{\rm VB}^{ZP}$	$\Delta\varepsilon_{\rm CB}^{ZP}$	$\Delta E_{\rm g}^{ZP}$	$\Delta\varepsilon_{\rm VB}^{ZP}$	$\Delta\varepsilon_{\rm CB}^{ZP}$	$\Delta E_{\rm g}^{ZP}$
Si	34.92	−8.019	−42.94	33.57	−8.603	−42.18
Silicene	52.28	−16.59	−68.87	51.30	−16.57	−67.87
Diamond	144.9	−263.3	−408.3	133.2	−274.1	−407.3
Graphite	693.7	56.05	−637.7	682.1	58.25	−623.9
Graphene	259.6	0.1830	−259.4	215.1	4.399	−210.7
z-BN	146.7	−174.8	−321.5	132.7	−182.3	−314.9
w-BN	120.0	−137.5	−257.5	113.9	−133.3	−247.2
h-BN	285.3	−160.2	−445.5	253.4	−154.7	−408.1
2D-BN	306.5	−203.7	−510.2	304.2	−164.9	−469.1

Our converged values for $\Delta E_{\rm g}^{ZP}(\Gamma)$ are within the acceptable range of variation (50 meV), based on differences in pseudopotential and **q**-mesh size. The results of the calculations are recorded in Tables I and II.

IV. RESULTS AND DISCUSSION

Having tested the convergence of $\Delta E_{\rm g}^{ZP}(\Gamma)$ for each of the considered structures, we discuss the effects of the zero-point renormalization on the electronic band structures. In addition, we compare the two Si allotropes, three C allotropes, and four BN polymorphs to demonstrate the effects of bulk crystal structure and dimen-

sionality on EPC induced renormalizations calculated in the adiabatic and nonadiabatic formulations of AHC theory. Our final values for $\Delta E_{\rm g}^{ZP}$ at the direct and indirect semiconductor gaps as well as the Dirac-points of graphene and silicene are given in Table II. Phonon dispersions were calculated in order to show that the relative magnitude of the phonon frequencies is related to the size of the ZPR at the electronic band gap. The temperature dependence of the eigenenergy renormalization was also considered, and temperature dependence profiles were calculated for the 3D and 2D materials using the adiabatic and nonadiabatic treatments of AHC theory. The parameters and result of our electronic structure calculations for each material are given in Appendix A.

A. Zero-point corrections of the electronic energy bands using the adiabatic and nonadiabatic calculations

We begin our discussion with Si, the most common and widely used semiconductor, which has a diamond cubic crystal structure. Our adiabatic calculations show the $\Delta\varepsilon_{n\mathbf{k}}$ for the conduction band (CB) edge and valence band (VB) edge at the Γ-point are −8.0 meV and 34.9 meV, respectively, leading to a direct $\Delta E_{\rm g}$ of −42.9 meV. We also note that $\Delta\varepsilon_{\rm CB}$ is negative, while $\Delta\varepsilon_{\rm VB}$ is positive, so that both $\Delta\varepsilon_{\rm CB}$ and $\Delta\varepsilon_{\rm VB}$ reduce the band gap. The nonadiabatic calculation gives $\Delta\varepsilon_{\rm CB} = -8.6$ and $\Delta\varepsilon_{\rm VB} = 33.6$ for a total renormalization of −42.2 meV, as summarized in Table I. The difference between the adiabatic and nonadiabatic renormalization values is only 0.8 meV or less than a thousandth of an eV. This suggests that the adiabatic approximation is appropriate for Si.

Table II gives the calculated $\Delta E_{\rm g}^{ZP}$ of Si for both its direct and indirect band gaps in the adiabatic and nonadiabatic formalisms. As mentioned before, the current adiabatic result of $\Delta E_{\rm g}^{ZP} = -63.6$ meV for the fundamental (indirect) band gap agrees well with experimental data[55] and previous predictions.[7] The value of the nonadiabatic renormalization at the fundamental gap is slightly smaller at −54.6 meV, but this is within the normal variation limits for this type of calculation. The calculated adiabatic value for the direct gap of Si, $\Delta E_{\rm g}^{ZP} = -42.9$ meV, is consistent with the value of −47.1 meV obtained by Poncé *et al.*[7] The nonadiabatic value of $\Delta E_{\rm g}^{ZP} = -42.2$ meV is also in agreement with Poncé *et al.*'s calculated value of 42.1 meV. An experimental study of the direct gap of Si was performed by Lautenschlager *et al.*[56], in which they examined the temperature dependence of critical points of Si's electronic band structure. Through fitting parameters, they determined the ZPR at the direct gap of Si to be 25 ± 17 meV(Table II). The upper range of this measurement is in relatively good agreement with our calculation.

For silicene, we have calculated the renormalization of the bands around the Fermi energy, $\Delta E_{\rm g}^{ZP}$. At the Γ-point we found $\Delta\varepsilon_{\rm CB} = -16.6$ meV and $\Delta\varepsilon_{\rm VB} = 52.3$ meV in the adiabatic formulations and $\Delta\varepsilon_{\rm CB} = -16.6$ meV and $\Delta\varepsilon_{\rm VB} = 51.3$ meV in the nonadiabatic formulation. Again, the difference in the total renormalization between the two formulations is minuscule at 1 meV (Table I), which indicates that the adiabatic approximation is sufficient to describe electron-phonon renormalizations in silicene. Table II summarizes the renormalization results at the Dirac-point. Here the cancellation of shifts in the CB and VB gives $\Delta E_{\rm g}^{ZP} = 0$.

Next we discuss ZPR in the C allotropes. As reported in I and II, the direct gap of diamond at the Γ-point has a $\Delta E_{\rm g}^{ZP}$ of −408.3 meV in adiabatic approximation and −407.3 meV with the nonadiabatic correction. The fundamental gap between Γ and $0.848X$ along the $\Gamma - X$ direction is $\Delta E_{\rm g}^{ZP} = -331.9$ meV and −329.3 meV in the adiabatic and nonadiabatic formulations respectively. These values are in excellent agreement with previous theory[7,17,29,30] and experimental data.[55]

When the crystal structure changes from diamond to hexagonal graphite, $\Delta E_{\rm g}^{ZP}(\Gamma)$ increases to −637.7 meV in the adiabatic approximation and −623.9 meV with the nonadiabatic correction. As summarized in Table I, the magnitude of the shift in the VB is almost twelve times larger than the shift in the CB at the Γ-point, and both $\Delta\varepsilon_{\rm CB}$ and $\Delta\varepsilon_{\rm VB}$ are positive, which is not seen in other the semiconductors calculated or silicene.

Surprisingly, for a single layer of graphite (i.e., graphene[60]) the magnitude of ΔE_{g}^{ZP} at the Γ-point is reduced by a factor of about 2.5, to −259.4 meV, in the adiabatic approximation and a factor of around 3, to −210.7, in the nonadiabatic formulation. We suspect this significant decrease in the magnitude of the renormalization at Γ is due to the interactions between the layers of graphite that are not present in graphene. However, like graphite, $\Delta\varepsilon_{\rm CB}$ and $\Delta\varepsilon_{\rm VB}$ in graphene are positive at the Γ-point and the main contribution to the total renormalization is from the VB, which suggests this may be a characteristic of the hexagonal C allotropes. Furthermore, in both graphite and graphene, $\Delta E_{g}^{ZP}(K-K)$ is 0.02 meV. This value for the renormalization is a numerical artifact further demonstrating the difficulty in the convergence of ZPR calculations, which is particularly delicate for the phonon frequencies at high symmetry points, other than Γ, with the Brillouin Zone. While spin-orbit coupling has been shown to open a small gap in graphene,[61] any opening of a band gap by EPC is prevented by the symmetry of the structure around the Fermi energy.[45] Again, in this work we focus on the gap at Γ of graphene and silicene to directly compare 3D and 2D materials; however, this methodology could be used to calculated renormalizations for modified graphene or allotropes of graphene with an opened gap at K.

It should also be noted that there is a substantial difference of 18.8% between the adiabatic and nonadiabatic calculations of $\Delta E_{\rm g}^{ZP}$ for graphene. The variation for the same calculations is only 2.2% in graphite and 0.25% in diamond. Based on this, the adiabatic approxima-

TABLE II. The calculated total ZPR (in meV) for energy bands around the Fermi energy of all nine materials studied in comparison with previous theoretical results (using FP DFT, DFPT, and Mote Carlo methods) and experimental data. The direct and indirect band gaps are given where appropriate as are the Dirac-points of silicene and graphene.

		Adiabatic		nonadiabatic		
Materials		Present	Other DFT	Present	Other DFT	exp.
Si	$\Gamma-\Gamma$	-42.94	-47.1[7]	-42.18	-42.1[7]	-25 ± 17[56]
			-44[31]			
	$\Gamma-0.848X$	-63.59	-64.3[7]	-54.55	-56.2[7]	-62[55]
			-57[31]			
			-60[57]			
Silicene	$\Gamma-\Gamma$	-68.87	–	-67.87	–	–
	$K-K$	0.000	–	0.000	–	–
Diamond	$\Gamma-\Gamma$	-408.3	-409[17]	-407.3	415.8[7]	-450[58]
			-439[7]			
			-436[29]			
			-404[30]			
			-430[59]			
			-615[13a]			
	$\Gamma-0.727X$	-331.9	-379.3[7]	-329.3	-329.8[7]	-364[55]
			-345[31]			
			-334[57]			
			-343[59]			
Graphite	$\Gamma-\Gamma$	-637.7	–	-623.9	–	–
	$K-K$	0.027	–	0.019	–	–
Graphene	$\Gamma-\Gamma$	-259.4	–	-210.7	–	–
	$K-K$	0.021	–	0.020	–	–
z-BN	$\Gamma-\Gamma$	-321.5	-388[29]	-314.9	-344[29]	–
					-502[7]	–
	$\Gamma-X$	-246.3	–	-221.9	-406[7]	–
w-BN	$\Gamma-\Gamma$	-257.5	–	-247.2	–	–
	$\Gamma-K$	-256.5	–	-239.4	–	–
h-BN	$\Gamma-\Gamma$	-422.5	–	-408.1	–	–
	$K-K$	-232.6	–	-217.6	–	–
2D-BN	$\Gamma-\Gamma$	-510.2	–	-469.1	–	–
	$K-K$	-472.2	–	-445.9	–	–

[a] This result was, at first, confirmed by an older QE+Yambo calculation that was later found to have a bug in its symmetry use at Γ[17].

tion fails for graphene, which has been previously confirmed by Pisana *et al.*[45] We also suspect that the adiabatic approximation is insufficient for ZPR convergence in graphite as well, due to its semimetallic properties.

In the four polymorphs of BN, the variation of $\Delta E_{\rm g}^{ZP}$ is much more gradual than it is for the C allotropes. Zincblende BN, also known as cubic boron nitride, is isoelectronic to diamond and has superior chemical stability.[62] Our adiabatic and nonadiabatic calculations yielded $\Delta E_{\rm g}^{ZP}(\Gamma) = -321.5$ meV and -314.9 meV, respectively. These results are in decent agreement (i.e. within 50 meV) with the prediction by Antonius *et al.*[29] The difference between the adiabatic and nonadiabatic results is about 2% at the Γ-point and 11% for the ZPR at the indirect gap, $\Delta E_{\rm g}^{ZP}(\Gamma - X)$. Poncé *et al.*[7] argued that a nonadiabatic treatment is necessary for polar materials, which have a non-zero Born effective charge. They showed that $\Delta E_{\rm g}^{ZP}$ at Γ diverges in the adiabatic approximation as the $\mathbf{q}$-mesh increases. This combined with the variation in the values yielded by the adiabatic and nonadiabatic treatments suggests that the nonadiabatic method is better suited in the case of z-BN.

Wurtzite BN is isoelectronic to Lonsdaleite (a.k.a hexagonal-diamond),[63] which is not included in this study due to its relative obscurity. Like z-BN, w-BN is a stable structure and is nearly as hard as diamond.[62] Its ZPR values are the smallest among the BN structures at $\Delta E_{\rm g}^{ZP}(\Gamma) = -257.5$ in the adiabatic approximation and $\Delta E_{\rm g}^{ZP}(\Gamma) = -247.2$ with the nonadiabatic correction, which have a variation of about 4%. The nonadiabatic ZPR at the indirect gap of w-BN is, likewise, about 7% smaller than its adiabatic counterpart.

Hexagonal BN is isoelectronic to graphite and is stable at ambient conditions.[62] Unlike semi-metallic graphite, however, h-BN is a wide-gap semiconductor. The adiabatic and nonadiabatic ZPR results for this structure are $\Delta E_{\rm g}^{ZP}(\Gamma) = -445.5$ meV and -408.1 meV, respectively. These two results differ by 8%, while ZPR's for the gap at K differ by 6% using adiabatic and nonadiabatic approximations, respectively. In both cases, the

more accurate nonadiabatic approximation reduces the magnitude of ZPR against the adiabatic approximation.

A structural analog to graphene, 2D-BN is a monolayer material with a hexagonal lattice and a large band gap whose $\Delta E_{\rm g}^{ZP}$ at the Γ-point was calculated to be −510.2 meV in the adiabatic approximation and −469.1 meV with a nonadiabatic treatment. This is the largest predicted ZPR among the BN materials, and the difference in the Γ-point renormalization between the adiabatic and the nonadiabatic results is 8%. The ZPR for the band gap at K is also sizable at K: $\Delta E_{\rm g}^{ZP}(K-K) = -445.9$ meV in the nonadiabatic formulation. Our treatments of the lattice calculations for each of the 2D materials is described in Appendix A. We note that recent studies indicate that spurious interactions from the periodic plane-wave calculations of 2D materials can effect electron-phonon calculations[64]. A truncated Coulomb interaction technique may be needed for future EPC calculations of 2D and 1D materials[64,65].

In each of the nine structures for which ZPR calculations have been performed, the nonadiabatic treatment always yielded smaller renormalizations at the band gap than the adiabatic treatment. For Si, silicene, and diamond the variations in $\Delta E_{\rm g}^{ZP}$ were minuscule and the Γ-point. For graphite, z-BN, and w-BN, the adiabatic and nonadiabatic calculations varied by roughly 7-10 meV, which is slightly larger than the variation in our convergence tests done using the nonadiabatic treatment(Fig. 1). In h-BN and 2D-BN, the difference in the two calculation methods is ∼ 40 meV with nonadiabatic ZPR's reduced by about 8% as compared to the adiabatic values. Graphene has the largest disparity, of nearly 50 meV, between its adiabatic and nonadiabatic renormalization calculations.

These results suggest that Si and diamond behave similarly. They are both non-polar semiconductors for which the zero-point electron-phonon renormalizations are consistently calculated in either the adiabatic or nonadiabatic treatments of AHC theory. Likewise, z-BN and w-BN have similar behaviors. Both are dense, wide-gap semiconductors with hardness comparable to diamond, and both are polar materials. The variations in their adiabatic and nonadiabatic ZPR at Γ are significant though not dramatic given that the differences only slightly exceed the variation seen in their convergence tests. For these materials, the nonadiabatic correction is important; however, the adiabatic approximation gives reasonable ZPR values that are within the expected variation[66] due to the use of different pseudopotential.[17] Following this trend, h-BN and 2D-BN have aspects consistent with expectations. Given that 2D-BN is essentially a single layer of h-BN, it is intuitive that the two structures would share similar EPC characteristics, especially since they are both semiconductors. This is confirmed, to a degree, by their Γ-point energy band shifts, which are close in magnitude (though 2D-BN has a much larger renormalization at the K-point than does h-BN). In addition, their adiabatic and nonadiabatic calculations vary by about 8% for both structures indicating that nonadiabatic corrections are necessary.

The exceptions are silicene, graphite, and graphene, which are also the semimetals. In the case of silicene, the unexpected element is the small difference between the adiabatic and nonadiabatic calculations. As it is a semimetal, we expected the ZPR convergence in the adiabatic approximation to fail for silicene. However, we have only performed ZPR convergence tests for the nonadiabatic treatment in this study. It may be necessary to examine the convergence of the adiabatic ZPR in silicene to gain a better understanding of its reaction to the adiabatic approximation as it applies to AHC theory. Graphite's outlying characteristic its relationship to graphene. Unlike their isoelectronic counterparts, h-BN and 2D-BN, graphite and graphene do not have similar ZPR magnitudes at Γ. The renormalization in graphite is considerably larger than it is in graphene. On the other hand, graphene and graphite have in common that both the $\Delta\varepsilon_{\rm CB}$ and $\Delta\varepsilon_{\rm VB}$ are positive resulting in a general upward shift of the energy bands, and the largest component of $\Delta E_{\rm g}^{ZP}(\Gamma)$ is from the VB. We also note that the adiabatic and nonadiabatic ZPR calculations for graphite are not drastically different as they are in graphene. While the nonadiabatic corrections are needed for an accurate treatment of both materials, the failure of the adiabatic approximation in graphene is apparent from the ZPR values alone.

Of the materials considered for this study, experimental data is currently only available for diamond and Si. As these structures have electron-phonon renormalizations that can be well described by the adiabatic approximation, it is difficult to assess, with the ZPR alone, whether or not the EPC properties of other materials are accurately calculated by the adiabatic or nonadiabatic treatments. Additional tests and calculations are typically needed for a thorough understanding of the approximation's validity. However, our renormalization calculations do indicate that the nonadiabatic corrections are more general as they do not contradict the results of the adiabatic approximation where it is known to be valid. From the ZPR calculations, we can also determine the relative significance of the EPC on the electronic structure. In 2D-BN, for example, the total ZPR of its indirect band gap is ∼ 0.45 eV, which is non-negligible for a material with $E_g = 4.64$eV. Save for Si and silicene, all of the other structures considered above exhibit significant EPC renormalizations to their electronic energy structures.

B. Phonon dispersions

To demonstrate the link between the electron-phonon renormalization and the phonon characteristic of various crystal structures, we have plotted phonon dispersions and phonon densities of state (DOS) for the Si allotropes in Figure 2, the C allotropes in Figure 3,

and the BN polymorphs in Figure 4. We find that the general trend that higher maximum optical phonon frequencies (wider phonon spectrum ranges) lead to stronger electron-phonon coupling and larger magnitudes for $\Delta E_g^{ZP}(\Gamma)$. For example, panels Figure 3(a) and Figure 3(b) indicate that the highest optical phonon frequency in graphite (~ 1600 cm^{-1}) is larger than that in diamond (~ 1300 cm^{-1}). Also, the $\Delta E_{g(\Gamma)}^{ZP}$ of graphite is larger than that of diamond. The situation is similar for the bulk BN polymorphs. Among them, h-BN has the highest maximum optical phonon frequency (~ 1450 cm^{-1}), while w-BN has the lowest (~ 1250 cm^{-1}), as seen in Figure 4 (a, b, and c). The Si allotropes follow the same pattern. Si has a slightly smaller phonon frequency range than silicene, and $\Delta E_g^{ZP}(\Gamma)$ for Si is roughly 25 meV smaller than it is for silicene. Additionally, Si and silicene have much narrower phonon frequency ranges than the C and BN materials, and their electron-phonon induced renormalizations are substantially smaller. Comparing bulk C allotropes and BN polymorphs, the trend that materials with higher maximum optical frequencies have larger ZPR magnitudes still, roughly, holds true. This observation is in line with the fact that stronger electron-phonon coupling is often caused by stronger atomic interactions.

Figure 5 maps out $\Delta E_g^{ZP}(\Gamma)$ as a function of frequency for the combined structures. Using this representation of the data, it is clear that there is a general trend toward larger absolute renormalization values as the phonon frequency range becomes wider. The notable outliers include 2D-BN and graphene. There is not enough evidence to determine if silicene is expressing behavior similar to graphene as the sample size of the Si allotropes is too small. It is possible that, due to its characteristic buckling, silicene may be showing characteristics of a 3D structure in this case. 3(b) and Figure 3(c) show that the phonon frequency ranges of graphite and graphene are similar, but $\Delta E_g^{ZP}(\Gamma)$ in graphene is about three times smaller in magnitude than that of graphite. This may be a result of differences in the EPC behavior due to the interlayer interactions in graphite that are absent in graphene. The opposite behavior is seen in h-BN and 2D-BN, however. Like graphite and graphene, the phonon frequency range of the two structures is comparable, but unlike the C allotropes, $\Delta E_g^{ZP}(\Gamma)$ for h-BN in slightly smaller (~ 60 meV) than that of 2D-BN. This may be an effect of the convergence of the ZPR calculations as the two numbers are not as dramatically different as they are with graphite and graphene. There is also the possibility that the deviation in 2D-BN from the behavior of the bulk BN materials is due to a lack of out-of-plane interactions. While we might expect graphene and 2D-BN to show similar outlying behavior if this were the case, the fact that graphene is a semimetal and 2D-BN is a semiconductor could explain the variation in their trends.

The evidence presented in the phonon dispersions and Figure 5 suggests that crystal structure in combination with phonon frequency data can be used to make rough predictions about the significance of electron-phonon induced renormalization of band gaps. The cubic structures, diamond, and z-BN are both dense stable materials with maximum phonon frequencies in the intermediate range of this data set, and we have calculated non-negligible band gap renormalizations for both. Si is isoelectronic to diamond and z-BN, but its frequency range is substantially smaller as is its calculated value of ΔE_g^{ZP}. The hexagonal layered structures, graphite, and h-BN, have the largest phonon frequency ranges that accompany significant ZPR values at Γ. Furthermore, ΔE_g^{ZP} for w-BN is the smallest of the BN polymorphs, which is consistent with its frequency range as compared to h-BN and z-BN. 2D-BN exhibits behavior that deviates slightly from the bulk materials. It also has a high maximum phonon frequency paired with a large ZPR, but its ΔE_g^{ZP} magnitude is larger than that of h-BN despite having a slightly lower optical phonon frequency range. Graphene is the most striking outlier. Despite having a phonon frequency range nearly identical to graphite, its ZPR is appreciably smaller. Given the many unique qualities of graphene, it is not surprising that its behavior, in this case, is also divergent. Further studies on the EPC in graphene would be useful to fully understand its differences from bulk and other 2D structures, such as an examination of the van der Waals interaction and a more in-depth dimensional analysis of carbon materials, including 1D structures.

C. Temperature-dependent band gaps

Having thoroughly analyzed the renormalizations of each considered structure at zero temperature, $T = 0$ K, it is instructive to perform calculations of the temperature dependence of those renormalizations. While zero-point motion in materials is significant and useful, many experiments and calculations are done at non-zero temperatures. As such, it is helpful to know how the eigenenergy renormalizations change as T increases.

We established that nonadiabatic corrections to the ZPR can be substantial depending on the material and crystal structure under consideration. The temperature dependent adiabatic and nonadiabatic renormalizations were also calculated for each structure to compare temperature trends and EPC characteristics for $T > 0$. Figure 6 shows the $\Delta E_g(\Gamma)$ temperature profiles for each structure with the nonadiabatic calculations in black and the adiabatic calculations in red. As expected from our previous ZPR results (Table I), Si, silicene, and diamond exhibit negligible differences between their adiabatic temperature profiles and their nonadiabatic corrections. For z-BN, w-BN, and 2D-BN the adiabatic and nonadiabatic renormalizations are closer in magnitude at temperatures below 300 K and diverge as T increases so that the difference between the treatments is more dramatic at high temperatures. For graphite, graphene, and h-BN

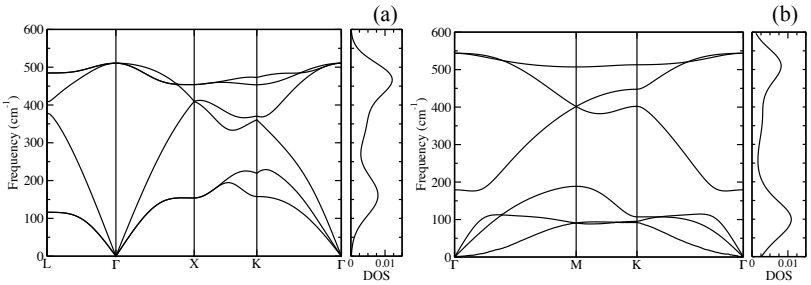

FIG. 2. The calculated phonon spectra and density of states for two Si allotropes: (a) Si and (b) silicene. The phonon density of states (DOS) is in unit of states/atom/cm^{-1}.

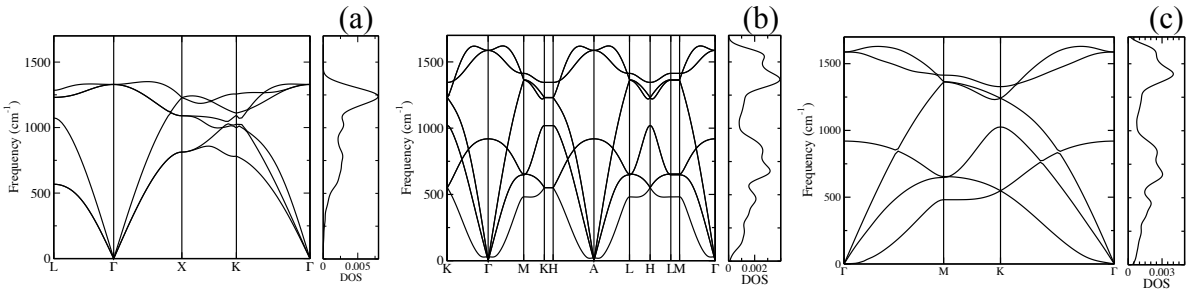

FIG. 3. The calculated phonon spectra and density of states for three C allotropes: (a) diamond, (b) graphite, and (c) graphene. The phonon density of states (DOS) is in unit of states/atom/cm^{-1}.

the nonadiabatic temperature profile is shifted uniformly such that the difference in values due to the correction is roughly the same at each temperature. Overall the nonadiabatic corrections do not have a dramatic effect on the relative temperature trends, so for our structural comparison, we will look at temperature profiles calculated with the nonadiabatic treatment.

The temperature (T) dependence of ΔE_g, calculated with nonadiabatic corrections, at the direct band gap is plotted for the Si allotropes, the C allotropes, and the BN polymorphs in Figure 7. The ΔE_g temperature profiles in most of these materials are similar: at low to room temperature, the ZPR dominates the total energy shift and $\Delta E_g(T)$ changes very gradually as a function of T. In these cases, one needs only consider phonon renormalization caused by the zero-temperature lattice vibrations up to room temperature. The exceptions to this are silicene and graphene, both of which have a more linear profile such that the magnitude of the renormalization steadily increases from the ZPR. This is particularly pronounced in silicene, which increases more than tenfold from 0 K to 1000 K, and at 300 K, the renormalization is no longer negligible at $\Delta E_g \sim 400$ meV. As this behavior is unique for our set of structures, silicene's buckled structure may be a contributing factor. The other 2D materials are flat and have no out-of-plane atomic interactions, and the bulk materials have consistent atomic interactions in all three directions. Silicene, on the other hand, has a slight deviation in its planar structure, and even though it is electronically stable, the EPC could be complicated by intricacies due to the slight out-of-plane buckling. This dramatic temperature profile may also be the result of a convergence issue. As our calculations for silicene were preliminary, further studies are required to explore the origins of its intense temperature dependence in the EPC induced renormalization.

At high temperatures ($T \gtrsim 400$ K), $\Delta E_g(T)$ increases dramatically as T rises in each of the structures. We also find that for bulk materials with a large ZPR, $\Delta E_g(T)$ increases slightly faster than it does in bulk materials with smaller ZPR's. The above can be easily understood by a simple Debye:[58]

$$\Delta E_{\rm g}(T) = -a\left[1 + \frac{2}{e^{\Theta/T} - 1}\right], \qquad (16)$$

where a and Θ are fitting parameters. When $T = 0$ in equation 16, the magnitude of $\Delta E_{\rm g}(T)$ is dependent on the magnitude of a. The larger a is, the faster $\Delta E_{\rm g}(T)$ will grow as T increases.

This is not the case for 2D materials, however, as is particularly clear in Figure 7(c) for h-BN and 2D-BN. The monolayer structure has a larger ZPR than the layered structure, but at $T \gtrsim 300$ K, ΔE_g for h-BN begins to increase more quickly than it does for 2D-BN. In the cases of silicene and graphene, it is more difficult to make a definitive statement about the relationship between the

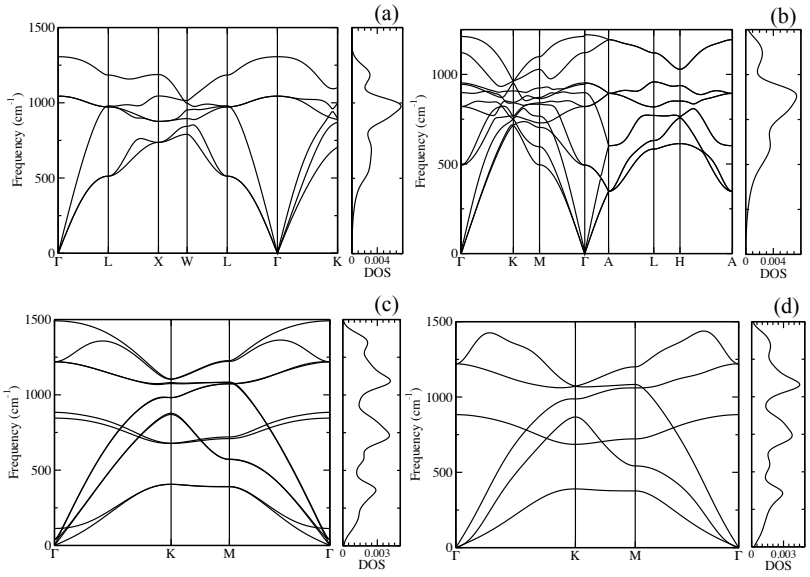

FIG. 4. The calculated phonon spectra and density of states (in unit of states/atom/cm^{-1}) for four BN polymorphs: z-BN (a), w-BN (b), h-BN (c), and 2D-BN (d).

ZPR and the temperature dependent rate of increase in the renormalization; however, a characteristic difference of the electron-phonon renormalization temperature dependence is indicated between the 2D and bulk materials.

V. CONCLUSIONS

We have investigated electron-phonon renormalization of eigenenergies in two Si allotropes, three C allotropes, and four BN polymorphs using DFPT. Our analysis demonstrates that $\Delta E_{\rm g}$ is sensitive to crystal structure and dimension and that it can be substantial in electronic structure calculations for some materials.This is the first direct comparison of eigenenergy renormalizations in isoelectronic structures as well as 3D and 2D materials. We discovered that the magnitudes of the total renormalization at the band gap, $\Delta E_{\rm g}^{ZP}(\Gamma)$, is directly related to the structural stiffness of a given 3D material. Low-dimensional structures such as planar 2D materials do not follow this trend indicating significant differences in their EPC behavior.

Very few first-principles calculations of phonon renormalization have been carried out because of their prohibitive computational cost. The major issue in these calculations is slow convergence, requiring extremely large and fine **q**-meshes. For these calculations, we have used the ABINIT package with Sternheimer equations.[27] Our calculations suggest that the ABINIT implementation converges relatively quickly, though it is highly memory intensive.

Analysis of the adiabatic and nonadiabatic treatments of AHC theory in ABINIT confirmed the conclusions of previous studies[7,67] that certain materials and crystal structures cannot be accurately described by the adiabatic, Born-Oppenheimer approximation.[41] Our results confirm that polar BN materials and semimetallic materials tend to have significant variations in their adiabatic and nonadiabatic ZPR's, suggesting a failure of the adiabatic approximation. Temperature-dependent $\Delta E_{\rm g}^{ZP}$ calculations also confirm that this disparity between the two treatments continues at higher temperatures. In different materials the adiabatic renormalizations have various deviations from the nonadiabatic results as temperature increases, indicating that the relative accuracy of adiabatic temperature dependent renormalization profiles is not reliable for all materials.

Next, we considered the ZPR values in concert with the phonon dispersions of each structure and found that bulk materials with wide phonon frequency ranges tend to have strong EPC and a sizable $\Delta E_{\rm g}$. These calculations suggest that high optical phonon frequency is a good indicator of whether or not the electron-phonon renormalization should be included in electronic structure calculations. However, this relationship does not always hold in monolayer structures, particularly graphene, where the magnitude of $\Delta E_{\rm g}$ is diminished compared to graphite even though the top optical phonon bands in graphene are located in roughly the same range as its layered counterpart. The departure from the behavior of the bulk structures may be a result of reduced DOS of the optical phonons in 2D materials, or, possibly, the absence of out-of-plane atomic interactions.

Our general observations of the behavior of electron-

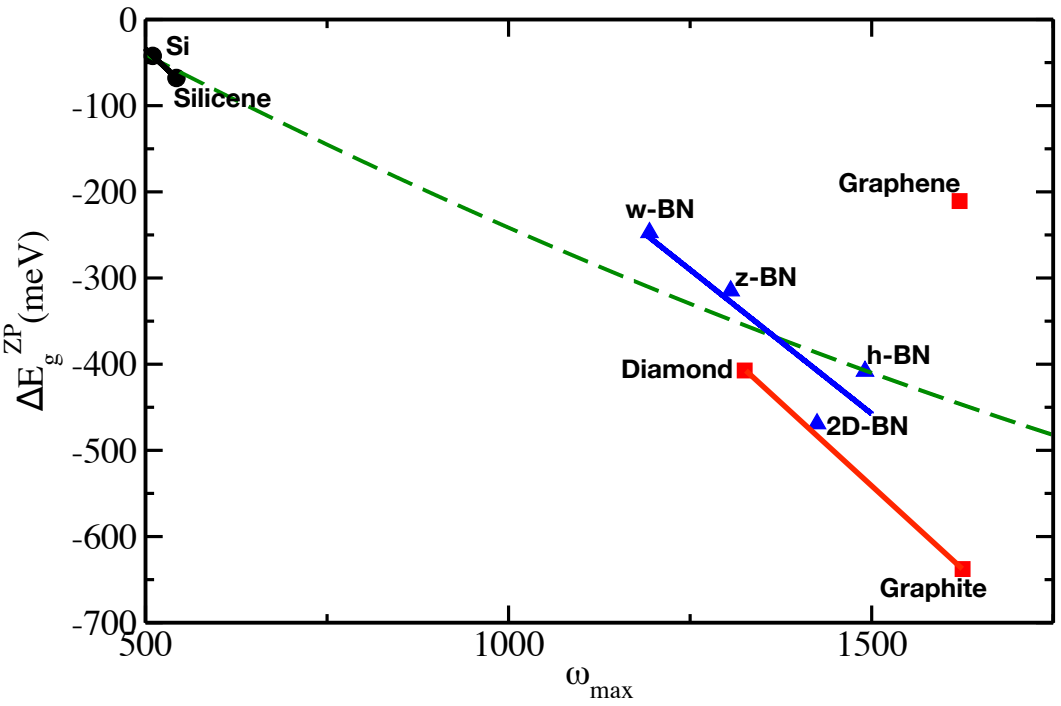

FIG. 5. $\Delta E_g^{ZP}(\Gamma)$ for each of the nine considered structures as a function of the phonon frequency range (ω_{max}). The black circles indicate the ZPR data for the two Si allotropes (Si and silicene), the red squares are the ZPR data for the C allotropes (diamond, graphite, and graphene), and the blue triangles are the ZPR data for the BN polymorphs (z-BN, w-BN, h-BN, and 2D-BN). The black, blue, and red lines are included group the Si, C and BN structures respectively, and the dashed green line is a visual guide of the rough trend over the entire set of materials. The Spearman Correlation coefficient for these data is $r_s = -0.733$, which indicates a relatively strong correlation between the highest optical frequencies and the renormalization values at Γ.

phonon energy band renormalizations in bulk materials tended to be contradicted by the 2D structures. EPC and ZPR have been previously shown to be enhanced in nanoscale structures;[8] however, here we find that the magnitude of ZPR is significantly reduced in graphene while it is slightly enhanced in 2D-BN and silicene. The temperature dependent profiles also indicate substantial differences between the 2D and 3D structures as temperature increases. Thus it is imperative and pertinent to study the effects of lattice vibrations and temperature dependence in 2D materials and nanostructures, including phonon-mediated electronic and optical properties. A thorough treatment of these nanostructures may also require considering a truncated Coulomb interaction technique to account for artificial couplings between periodic images of 1D and 2D materials.

ACKNOWLEDGMENTS

This work was supported by U.S. DOE Early Career Award (Grant No. DE-SC0006433) and the startup funding from Colorado School of Mines (CSM). Computations were carried out at the Golden Energy Computing Organization at CSM and the National Energy Research Scientific Computing Center (NERSC). ZW thanks M. Lusk and D. Wood for their insightful discussions.

Appendix A: Electronic structures

Relaxed lattice constants and electronic band structures were calculated for the structures described above. The methodology and computational parameters are discussed in section II C. In Table III the lattice constants are listed with comparisons to previous theoretical results and experimental data, and our calculations are in good agreement. The interlayer distances for the 2D structures were optimized and found to be 2.0 nm for silicene, 1.8 nm for graphene, and 1.7 nm for 2D-BN, and the buckled separation, Δ_0, for silicene was predicted to be 0.443 Å. As mentioned in section II C, van der Waals corrections to the exchange-correlation energy (vdw-DFT-D3(BJ)[52,53]) were considered for graphite and graphene. The calculated out of plane lattice constants with this correction are very close to the experimental values;[54,68] without the van der Waals correction, $c/a = 3.45$ for graphite, which is consistent with previous

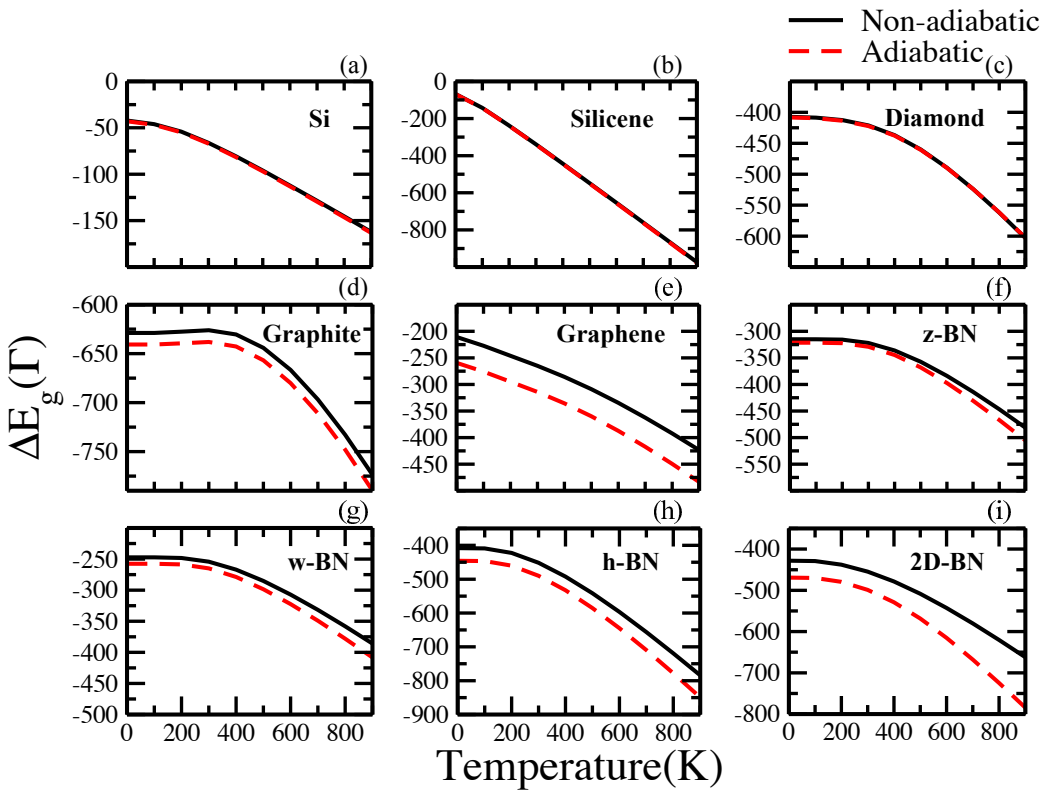

FIG. 6. The adiabatic and nonadiabatic electron-phonon renormalizations of $\Delta E_{\rm g}^{ZP}(\Gamma)$ as a function of temperature for (a) Si, (b) silicene, (c) diamond, (d) graphite, (e) graphene, (f) z-BN, (g) w-BN, (h) h-BN, and (i) 2D-BN. The nonadiabatic calculations are denoted by the solid black curves, and the adiabatic calculations are given by the dashed red curves.

DFT calculations.[51] Our EPC computations were done using the theoretical equilibrium structures calculated in Table III. Changes in $\Delta\varepsilon_{n\mathbf{k}}$ due to small variations in lattice constants compared with measured parameters are expected to be negligible (less than a few percents).

For this study, we have considered isoelectronic structures with different elemental compositions. For example, Si, diamond, and z-BN all have diamond crystal structures; silicene, graphene, and 2D-BN all have planar hexagonal structures; and graphite and h-BN both have layered hexagonal structures.

Despite their similar symmetries, these materials have notable differences in their electronic characteristics. Si, diamond, z-BN, w-BN, h-BN, and 2D-BN are standard (in the case of Si) or wide-gap semiconductors. On the other hand, graphite, graphene, and silicnene are semimetals, so we anticipate that the EPC characteristics in these materials may differ notably. We have included calculations of silicene, graphene, and graphite for continuity in our isoelectronic comparisons as well as to compare 3D and 2D structures of similar crystal symmetries. Given that these materials are not semiconductors, we will focus our calculations on the gap in the bandstructure at the Γ-point. While we have also considered the Dirac points at K in both silicene and graphene, they are not significant to our comparisons in later sections. Table IV summarizes the direct and indirect band gaps for the semiconducting materials. Our results are in good agreement with those of previous DFT calculations, which are known to underestimate the band gap as compared to experimental data.

The band structures and densities of state for each material are given in Figures 8, 9, and 10. Si and silicene are shown in Figure 8. In addition to being the most widely used semiconducting material, Si is also one of the few materials for which there have been experimental measurements done of the ZPR at the indirect band gap, making it a useful structure for comparison in this and similar studies.[55] Silicene is reminiscent of graphene with its similar Dirac point at K as well as its hexagonal symmetry, and it is thought to share many of graphene's electronic properties.[72,73] However, silicene differs from graphene, as well as 2D-BN, in that it is not flat. Due to sp^2-sp^3 hybridization, free-standing silicene has a buckled honeycomb structure, making it a quasi-2D structure.[73] Furthermore, free-standing silicene is not likely to be able to exist naturally. It is typically deposited on a metallic substrate, which changes its lattice parameters slightly for experimental studies.[72]

The electronic dispersions of the carbon allotropes are

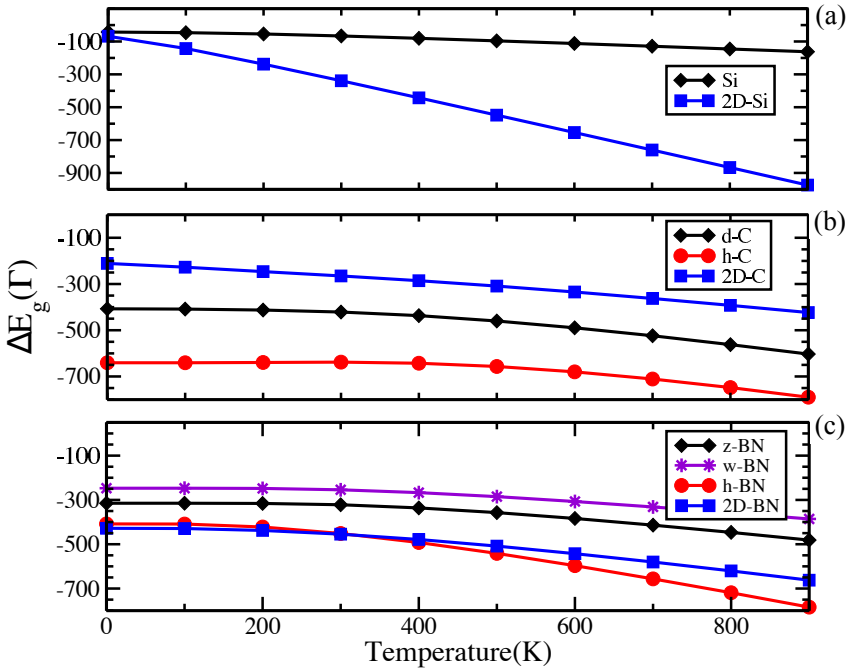

FIG. 7. The electron-phonon renormalization at the Γ-point as a function of temperature for (a) Si and silicene(2D-Si); (b) diamond(d-C), graphite(h-C), and graphene(2D-C); and (c) z-BN, w-BN, h-BN, and 2D-BN.

TABLE III. Lattice constants (in Å), calculated using GGA-PBE[48] pseudopotentials. Current values are compared to previous theoretical results and experimental data. In the case of silicene, Δ_0 is the relaxed buckled separation. The interlayer distances for the 2D structures are 20Å, 18Å, and 17Å for silicene, graphene, and 2D-BN respectively.

Material	Present Calculation	Previous theory	Experiment
Silicon	5.465	5.475[69]	5.430[69]
Silicene	3.870	3.830[70]	3.850[71]
	Δ_0=0.443	Δ_0=0.440[70]	Δ_0=0.47[72,73]
Diamond	3.576	3.576[69]	3.567[69]
Graphite	$a = 2.458$	$a = 2.460$[54]	$a = 2.462$[68]
	$c/a = 2.725$	$c/a = 2.740$[54]	$c/a = 2.725$[68]
Graphene	$a = 2.458$	$a = 2.460$[51]	$a = 2.462$[68]
z-BN	3.620	3.621[74]	3.615[75]
w-BN	$a = 2.572$	$a = 2.542$[76]	$a = 2.550$[62]
	$c/a = 1.652$	$c/a = 1.630$[76]	$c/a = 1.630$[62]
h-BN	$a = 2.508$	$a = 2.511$[76]	$a = 2.504$[62]
	$c/a = 2.674$	$c/a = 2.660$[76]	$c/a = 2.660$[62]
2D-BN	$a = 2.508$	$a = 2.511$[76]	$a = 2.504$[62]

shown in Figure 9. Of these structures, only diamond is a semiconductor with a wide indirect band gap calculated to be 4.233 eV (Table IV). Graphite and graphene are considered semimetals as they have a zero band gap but do not share the electronic properties of true metals. Graphite, for instance, has strong in-plane bonds but weak, van der Waals dominated, interactions between each layer.[51] In its single layer allotrope, graphite is known as graphene, which is the most famous and broadly studied of the 2D structures. Its zero band gap associated with the relativistic Dirac fermions at the K point in the BZ, make it unfeasible for optoelectronic applications in its unaltered form.[82] Graphene is, however, prevalent in a wide range of EPC based studies including superconductivity,[83–85] nonadiabatic vibrational frequencies,[44,45] and GW corrections to electron-phonon matrix elements.[86]

Figure 10 shows our calculations of the electronic band

TABLE IV. The electronic band gaps, in units of electron volts, of each of the semiconducting materials: Si, diamond, z-BN, w-BN, h-BN, and 2D-BN.

	Direct Gap (eV)				Indirect Gap (eV)			
Material	Gap	Present	other DFT	exp.	Gap	Present	other DFT	exp.
Si	$\Gamma-\Gamma$	2.568	2.56[74]	3.378[77]	Γ-0.848X	0.607	0.612[74]	1.17[77]
Diamond	$\Gamma-\Gamma$	5.583	5.57[74]	7.3[55]	Γ-0.727X	4.233	4.113[74]	5.48[55]
z-BN	$\Gamma-\Gamma$	8.850	8.70[78]	14.5[79]	Γ-X	4.440	4.45[74]	6.4[79]
w-BN	$\Gamma-\Gamma$	8.150	8.0[78]	-	Γ-K	5.290	5.81[78]	-
h-BN	$\Gamma-\Gamma$	6.560	-	-	0.92K-M	4.620	4.5[78]	5.971[80]
2D-BN	$\Gamma-\Gamma$	6.340	-	-	-	-	-	-
	K-K	4.640	4.64[76]	5.5[81]	-	-	-	-

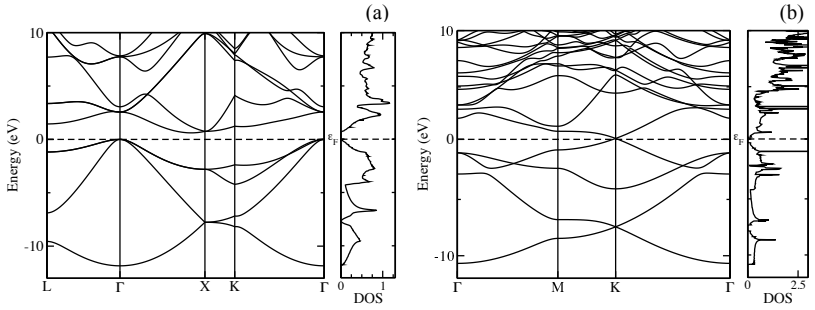

FIG. 8. The electronic band structures and densities of state for Si (a) and silicene (b). The DOS is given in units of states/eV/bohr^3. Zero energy is set at the valence band maximum and ε_F indicates the Fermi energy.

structures and DOS for the four BN polymorphs. Boron nitride can exist in various crystal configurations, but its default form is the layered hexagonal structure, h-BN, which consists of layers of flat sheets governed by sp^2 bonds between boron and nitrogen atoms. Large out-of-plane distances separate each layer resulting in a lower density structure. Conversely, zincblende BN, also known as cubic BN, is second only to diamond in hardness. It is constructed from sp^3 bonds, which make is denser and harder than h-BN. In addition, z-BN is chemically inert, has a high thermal conductivity and a low dielectric constant, as well as a wide band gap.[87] Like z-BN, w-BN has sp^3 bonds and a higher density structure than h-BN. 2D-BN is the single layer polymorph of h-BN and has the same honeycomb structure seen in graphene, though, unlike graphene, 2D-BN is a wide gap semiconductor.[76] BN crystals do not occur naturally, however, h-BN has been synthesized and transformed, through pressure, into its denser polymorphs (z-BN and w-BN),[88,89] as well as isolated to extract single layers, forming 2D-BN.[81]

* zhiwu@mines.edu

[1] F. Giustino, Review of Modern Physics **89**, 1 (2017).

[2] M. S. Hybertsen and S. G. Louie, Phys. Rev. B **34**, 5390 (1986).

[3] W. G. Aulbur, L. Jnsson, and J. W. Wilkins (Academic Press, 2000), vol. 54 of *Solid State Physics*, pp. 1 – 218, URL http://www.sciencedirect.com/science/article/pii/S0081194708602489.

[4] G. Onida, L. Reining, and A. Rubio, Rev. Mod. Phys. **74**, 601 (2002).

[5] P. Hohenberg and W. Kohn, Phys. Rev. **136**, B864 (1964), URL http://link.aps.org/doi/10.1103/PhysRev.136.B864.

[6] W. Kohn and L. J. Sham, Phys. Rev. **140**, A1133 (1965), URL http://link.aps.org/doi/10.1103/PhysRev.140.A1133.

[7] S. Poncé, Y. Gillet, J. Laflamme Janssen, A. Marini, M. Verstraete, and X. Gonze, J. Chem. Phys. **143**, 102813 (2015), URL http://scitation.aip.org/content/aip/journal/jcp/143/10/10.1063/1.4927081.

[8] A. Franceschetti, Phys. Rev. B **76**, 161301 (2007), URL http://link.aps.org/doi/10.1103/PhysRevB.76.161301.

[9] P. B. Allen and M. Cardona, Phys. Rev. B **23**, 1495 (1981).

[10] P. B. Allen and M. Cardona, Phys. Rev. B **27**, 4760 (1983).

[11] F. Giustino, M. L. Cohen, and S. G. Louie, Phys. Rev. B **76**, 165108 (2007).

[12] A. Marini, Phys. Rev. Lett. **101**, 106405 (2008), URL http://link.aps.org/doi/10.1103/PhysRevLett.101.106405.

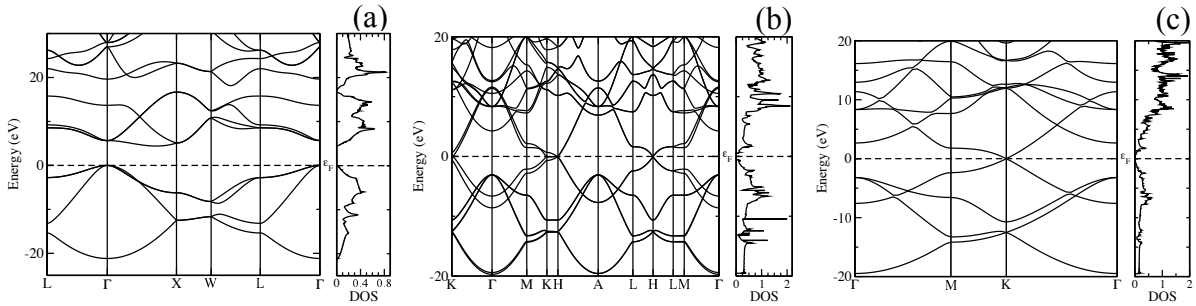

FIG. 9. The electronic band structures and densities of state for diamond (a), graphite (b), and graphene(c). The DOS is given in units of states/eV/bohr^3. Zero energy is set at the valence band maximum and ε_F indicates the Fermi energy.

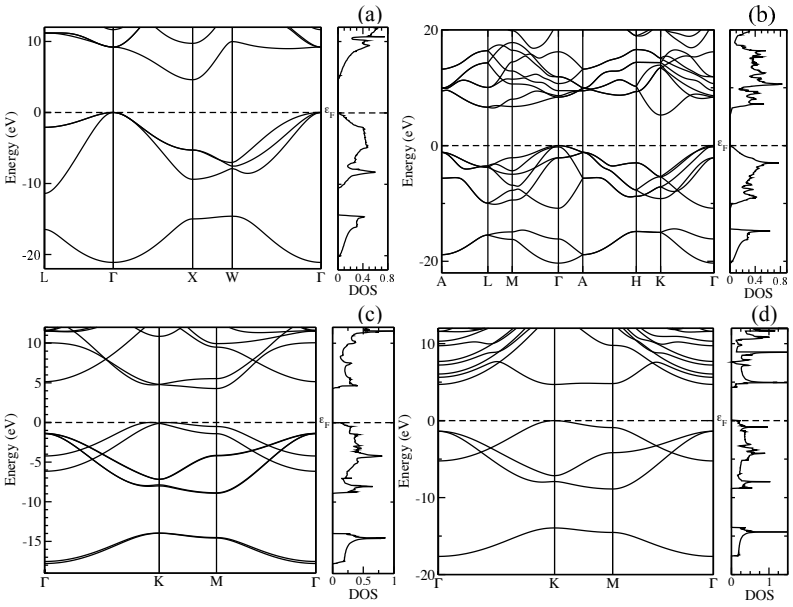

FIG. 10. The electronic band structures and densities of state for z-BN (a), w-BN (b), h-BN (c), and 2D-BN (d). The DOS is given in units of states/eV/bohr^3. Zero energy is set at the valence band maximum and ε_F indicates the Fermi energy.

[13] F. Giustino, S. G. Louie, and M. L. Cohen, Phys. Rev. Lett. **105**, 265501 (2010).

[14] X. Gonze, P. Boulanger, and M. Ct, Annalen der Physik **523**, 168 (2011), ISSN 1521-3889, URL http://dx.doi.org/10.1002/andp.201000100.

[15] E. Cannuccia and A. Marini, Phys. Rev. Lett. **107**, 255501 (2011), URL http://link.aps.org/doi/10.1103/PhysRevLett.107.255501.

[16] Cannuccia, E. and Marini, A., Eur. Phys. J. B **85**, 320 (2012), URL http://dx.doi.org/10.1140/epjb/e2012-30105-4.

[17] S. Poncé, G. Antonius, P. Boulanger, E. Cannuccia, A. Marini, M. Cote, and X. Gonze, Comput. Mater. Sci. **83**, 341 (2014).

[18] S. Poncé, G. Antonius, Y. Gillet, P. Boulanger, J. L. Janssen, A. Marini, M. Cote, , and X. Gonze, Phys. Rev. B **90**, 214304 (2014).

[19] S. Baroni, S. de Gironcoli, A. Dal Corso, and P. Giannozzi, Rev. Mod. Phys. **73**, 515 (2001), URL http://link.aps.org/doi/10.1103/RevModPhys.73.515.

[20] X. Gonze, Phys. Rev. B **55**, 10337 (1997).

[21] P. B. Allen and V. Heine, J. Phys. C: Solid State Physics **9**, 2305 (1976).

[22] N. Marzari, A. A. Mostofi, J. R. Yates, I. Souza, and D. Vanderbilt, Rev. Mod. Phys. **84**, 1419 (2012).

[23] P. Giannozzi, S. Baroni, N. Bonini, M. Calandra, R. Car, C. Cavazzoni, D. Ceresoli, G. L. Chiarotti, M. Cococcioni, I. Dabo, et al., J. Phys.: Condens. Matt. **21**, 395502 (2009), URL http://www.quantum-espresso.org.

[24] A. A. Mostofi, J. R. Yates, Y.-S. Lee, I. Souza, D. Vanderbilt, and N. Marzari, Comput. Phys. Commun. **178**, 685 (2008).

[25] S. Poncé, E. Margine, C. Verdi, and F. Giustino, Computer Physics Communications **209**, 116 (2016), ISSN 0010-4655, URL http://www.sciencedirect.com/science/article/pii/S0010465516302260.

[26] X. Gonze, J.-M. Beuken, R. Caracas, F. Detraux, M. Fuchs, G.-M. Rignanese, L. Sindic, M. Ver-

straete, G. Zerah, F. Jollet, et al., Computational Materials Science **25**, 478 (2002), ISSN 0927-0256, URL http://www.sciencedirect.com/science/article/pii/S0927025602003257.
[27] R. M. Sternheimer, Phys. Rev. **96**, 951 (1954), URL https://link.aps.org/doi/10.1103/PhysRev.96.951.
[28] A. Marini, C. Hogan, M. Grning, and D. Varsano, Comput. Phys. Commu. **180**, 1392 (2009).
[29] G. Antonius, S. Poncé, E. Lantagne-Hurtubise, G. Auclair, X. Gonze, and M. Côté, Phys. Rev. B **92**, 085137 (2015), URL http://link.aps.org/doi/10.1103/PhysRevB.92.085137.
[30] G. Antonius, S. Poncé, P. Boulanger, M. Cote, and X. Gonze, Phys. Rev. Lett. **112**, 215501 (2014).
[31] M. Zacharias and F. Giustino, Phys. Rev. B **94**, 075125 (2016), URL https://link.aps.org/doi/10.1103/PhysRevB.94.075125.
[32] F. E. Williams, Phys. Rev. **82**, 281 (1951), URL https://link.aps.org/doi/10.1103/PhysRev.82.281.2.
[33] M. Lax, The Journal of Chemical Physics **20**, 1752 (1952), https://doi.org/10.1063/1.1700283, URL https://doi.org/10.1063/1.1700283.
[34] C. Faber, J. L. Janssen, M. Côté, E. Runge, and X. Blase, Phys. Rev. B **84**, 155104 (2011), URL https://link.aps.org/doi/10.1103/PhysRevB.84.155104.
[35] B. Monserrat, Phys. Rev. B **93**, 100301 (2016), URL https://link.aps.org/doi/10.1103/PhysRevB.93.100301.
[36] H. Y. Fan, Phys. Rev. **82**, 900 (1951), URL http://link.aps.org/doi/10.1103/PhysRev.82.900.
[37] A. B. Migdal, Sov. Phys. JETP (1958).
[38] M. Cardona, T. A. Meyer, and M. L. W. Thewalt, Phys. Rev. Lett. **92**, 196403 (2004), URL https://link.aps.org/doi/10.1103/PhysRevLett.92.196403.
[39] S. Engelsberg and J. R. Schrieffer, Phys. Rev. **131**, 993 (1963), URL https://link.aps.org/doi/10.1103/PhysRev.131.993.
[40] J. R. Schrieffer, *Theory of Superconductivity* (W. A. Benjamin, Inc., Publishers, 1964).
[41] M. Born and R. Oppenheimer, Annalen der Physik **389**, 457 (1927), ISSN 1521-3889, URL http://dx.doi.org/10.1002/andp.19273892002.
[42] A. M. Saitta, M. Lazzeri, M. Calandra, and F. Mauri, Phys. Rev. Lett. **100**, 226401 (2008), URL https://link.aps.org/doi/10.1103/PhysRevLett.100.226401.
[43] M. Calandra, G. Profeta, and F. Mauri, Phys. Rev. B **82**, 165111 (2010), URL https://link.aps.org/doi/10.1103/PhysRevB.82.165111.
[44] M. Lazzeri and F. Mauri, Phys. Rev. Lett. **97**, 266407 (2006), URL https://link.aps.org/doi/10.1103/PhysRevLett.97.266407.
[45] S. Pisana, M. Lazzeri, C. Casiraghi, K. S. Novoselov, A. K. Geim, A. C. Ferrari, and F. Mauri, Nature Materials **6**, 198201 (2007), URL http://www.nature.com/nmat/journal/v6/n3/full/nmat1846.html?foxtrotcallback=true.
[46] N. Caudal, A. M. Saitta, M. Lazzeri, and F. Mauri, Phys. Rev. B **75**, 115423 (2007), URL https://link.aps.org/doi/10.1103/PhysRevB.75.115423.
[47] S. Piscanec, M. Lazzeri, J. Robertson, A. C. Ferrari, and F. Mauri, Phys. Rev. B **75**, 035427 (2007), URL https://link.aps.org/doi/10.1103/PhysRevB.75.035427.
[48] J. P. Perdew, K. Burke, and M. Ernzerhof, Phys. Rev. Lett. **77**, 3865 (1996), URL http://link.aps.org/doi/10.1103/PhysRevLett.77.3865.
[49] N. Troullier and J. L. Martins, Phys. Rev. B **43**, 1993 (1991), URL http://link.aps.org/doi/10.1103/PhysRevB.43.1993.
[50] M. Fuchs and M. Scheffler, Computer Physics Communications **119**, 67 (1999), ISSN 0010-4655, URL http://www.sciencedirect.com/science/article/pii/S001046559800201X.
[51] N. Mounet and N. Marzari, Phys. Rev. B **71**, 205214 (2005).
[52] S. Grimme, J. Antony, S. Ehrlich, and H. Krieg, The Journal of Chemical Physics **132**, 154104 (2010), http://dx.doi.org/10.1063/1.3382344, URL http://dx.doi.org/10.1063/1.3382344.
[53] S. Grimme, S. Ehrlich, and L. Goerigk, Journal of Computational Chemistry **32**, 1456 (2011), ISSN 1096-987X, URL http:https://doi.org/10.1002/jcc.21759.
[54] B. Van Troeye, M. Torrent, and X. Gonze, Phys. Rev. B **93**, 144304 (2016), URL https://link.aps.org/doi/10.1103/PhysRevB.93.144304.
[55] M. Cardona and M. L. W. Thewalt, Rev. Mod. Phys. **77**, 1173 (2005).
[56] P. Lautenschlager, M. Garriga, L. Vina, and M. Cardona, Phys. Rev. B **36**, 4821 (1987), URL https://link.aps.org/doi/10.1103/PhysRevB.36.4821.
[57] B. Monserrat and R. J. Needs, Phys. Rev. B **89**, 214304 (2014), URL https://link.aps.org/doi/10.1103/PhysRevB.89.214304.
[58] S. Logothetidis, J. Petalas, H. M. Polatoglou, and D. Fuchs, Phys. Rev. B **46**, 3376 (1992).
[59] J. H. Lloyd-Williams and B. Monserrat, Phys. Rev. B **92**, 184301 (2015), URL https://link.aps.org/doi/10.1103/PhysRevB.92.184301.
[60] K. S. Novoselov, A. K. Geim, S. V. Morozov, D. Jiang, Y. Zhang, S. V. Dubonos, I. V. Grigorieva, and A. A. Firsov, Science **306**, 666 (2004), URL http://science.sciencemag.org/content/306/5696/666.
[61] Y. Yao, F. Ye, X.-L. Qi, S.-C. Zhang, and Z. Fang, Phys. Rev. B **75**, 041401 (2007), URL http://link.aps.org/doi/10.1103/PhysRevB.75.041401.
[62] K. T. Park, K. Terakura, and N. Hamada, J. Phys. C: Solid State Phys. **20**, 1241 (1987).
[63] A. De and C. E. Pryor, Journal of Physics: Condensed Matter **26**, 045801 (2014), URL http://stacks.iop.org/0953-8984/26/i=4/a=045801.
[64] T. Sohier, M. Calandra, and F. Mauri, Phys. Rev. B **94**, 085415 (2016), URL https://link.aps.org/doi/10.1103/PhysRevB.94.085415.
[65] C. A. Rozzi, D. Varsano, A. Marini, E. K. U. Gross, and A. Rubio, Phys. Rev. B **73**, 205119 (2006), URL https://link.aps.org/doi/10.1103/PhysRevB.73.205119.
[66] Note1, this is true for calculations using a substantial broadening parameter, such as $i\eta = 100$, to speed convergence (see Antonius *et. al.*[29]). The convergence tests done by Poncé *et al.*[7] indicate divergence in $\Delta E_{\mathrm{g}}^{ZP}$ for increasing N_q, which suggests that the nonadiabatic corrections to the ZPR are necessary for any material with a non-zero Born effective charge.
[67] S. Pisana, M. Lazzeri, C. Casiraghi, K. S. Novoselov, A. K. Geim, A. C. Ferrari, and F. Mauri, Nature Mater. **6**, 198 (2007), URL http://dx.doi.org/10.1038/nmat1846.
[68] Y. X. Zhao and I. L. Spain, Phys. Rev. B **40**, 993 (1989), URL https://link.aps.org/doi/10.1103/PhysRevB.40.993.

[69] Z. Wu and R. E. Cohen, Phys. Rev. B **73**, 235116 (2006).

[70] J.-A. Yan, S.-P. Gao, R. Stein, and G. Coard, Phys. Rev. B **91**, 245403 (2015), URL https://link.aps.org/doi/10.1103/PhysRevB.91.245403.

[71] S. Cahangirov, V. O. Özçelik, L. Xian, J. Avila, S. Cho, M. C. Asensio, S. Ciraci, and A. Rubio, Phys. Rev. B **90**, 035448 (2014), URL https://link.aps.org/doi/10.1103/PhysRevB.90.035448.

[72] J. Zhu and U. Schwingenschlgl, ACS Applied Materials & Interfaces **6**, 11675 (2014), http://dx.doi.org/10.1021/am502469m, URL http://dx.doi.org/10.1021/am502469m.

[73] P. Vogt, P. De Padova, C. Quaresima, J. Avila, E. Frantzeskakis, M. C. Asensio, A. Resta, B. Ealet, and G. Le Lay, Phys. Rev. Lett. **108**, 155501 (2012), URL https://link.aps.org/doi/10.1103/PhysRevLett.108.155501.

[74] A. Jain, S. P. Ong, G. Hautier, W. Chen, W. D. Richards, S. Dacek, S. Cholia, D. Gunter, D. Skinner, G. Ceder, et al., APL Materials **1**, 011002 (2013), URL http://dx.doi.org/10.1063/1.4812323.

[75] T. Sma, A. Sawaoka, and S. Saito, Materials Research Bulletin **9**, 755 (1974), ISSN 0025-5408, URL http://www.sciencedirect.com/science/article/pii/002554087490110X.

[76] M. Topsakal, E. Aktürk, and S. Ciraci, Phys. Rev. B **79**, 115442 (2009), URL http://link.aps.org/doi/10.1103/PhysRevB.79.115442.

[77] G. E. Jellison and F. A. Modine, Phys. Rev. B **27**, 7466 (1983), URL https://link.aps.org/doi/10.1103/PhysRevB.27.7466.

[78] Y.-N. Xu and W. Y. Ching, Phys. Rev. B **44**, 7787 (1991), URL https://link.aps.org/doi/10.1103/PhysRevB.44.7787.

[79] R. Chrenko, Solid State Communications **14**, 511 (1974), ISSN 0038-1098, URL http://www.sciencedirect.com/science/article/pii/0038109874909788.

[80] K. Watanabe, T. Taniguchi, and H. Kanda, Nature Materials **3**, 404 (2004), URL http://mines.idm.oclc.org/login?url=https://search.proquest.com/docview/222758837?accountid=25386.

[81] L. Song, L. Ci, H. Lu, P. B. Sorokin, C. Jin, J. Ni, A. G. Kvashnin, D. G. Kvashnin, J. Lou, B. I. Yakobson, et al., Nano Letters **10**, 3209 (2010), http://dx.doi.org/10.1021/nl1022139, URL http://dx.doi.org/10.1021/nl1022139.

[82] D. M., O. W., and W. Z., Scientific Reports **3**, 2289 (2013), URL https://www.ncbi.nlm.nih.gov/pmc/articles/PMC3724180/.

[83] E. R. Margine and F. Giustino, Phys. Rev. B **90**, 014518 (2014), URL https://link.aps.org/doi/10.1103/PhysRevB.90.014518.

[84] J.-J. Zheng and E. R. Margine, Phys. Rev. B **94**, 064509 (2016), URL https://link.aps.org/doi/10.1103/PhysRevB.94.064509.

[85] E. R. Margine, H. Lambert, and F. Giustino, Scientific Reports **6**, 21424 (2016), URL https://www.nature.com/articles/srep21414.

[86] M. Lazzeri, C. Attaccalite, L. Wirtz, and F. Mauri, Phys. Rev. B **78**, 081406 (2008), URL https://link.aps.org/doi/10.1103/PhysRevB.78.081406.

[87] W. J. Yu, W. M. Lau, S. P. Chan, Z. F. Liu, and Q. Q. Zheng, Phys. Rev. B **67**, 014108 (2003), URL https://link.aps.org/doi/10.1103/PhysRevB.67.014108.

[88] R. H. W. Jr., The Journal of Chemical Physics **34**, 809 (1961), http://dx.doi.org/10.1063/1.1731679, URL http://dx.doi.org/10.1063/1.1731679.

[89] F. P. Bundy and R. H. W. Jr., The Journal of Chemical Physics **38**, 1144 (1963), http://dx.doi.org/10.1063/1.1733815, URL http://dx.doi.org/10.1063/1.1733815.